

Evidence of Two-Source King Plot Nonlinearity in Spectroscopic Search for New Boson

Joonseok Hur^{1,*}, Diana P.L. Aude Craik^{1,*}, Ian Counts^{1,*}, Eugene Knyazev¹, Luke Caldwell², Calvin Leung¹, Swadha Pandey¹, Julian C. Berengut³, Amy Geddes³, Witold Nazarewicz⁴, Paul-Gerhard Reinhard⁵,

Akio Kawasaki⁶, Honggi Jeon⁷, Wonho Jhe⁷ and Vladan Vuletić^{1,†}

¹*Department of Physics and Research Laboratory of Electronics, Massachusetts Institute of Technology, Cambridge, Massachusetts 02139, USA*

²*JILA, NIST and University of Colorado, Boulder, Colorado 80309, USA*

³*School of Physics, University of New South Wales, Sydney, New South Wales 2052, Australia*

⁴*Facility for Rare Isotope Beams and Department of Physics and Astronomy, Michigan State University, East Lansing, Michigan 48824, USA*

⁵*Institut für Theoretische Physik, Universität Erlangen, Erlangen D-91054, Germany*

⁶*National Metrology Institute of Japan (NMIJ), National Institute of Advanced Industrial Science and Technology (AIST), 1-1-1 Umezono, Tsukuba, Ibaraki 305-8563, Japan*

⁷*Department of Physics and Astronomy, Seoul National University, Seoul 151-747, Korea*

 (Received 8 January 2022; revised 19 February 2022; accepted 2 March 2022; published 22 April 2022)

Optical precision spectroscopy of isotope shifts can be used to test for new forces beyond the standard model, and to determine basic properties of atomic nuclei. We measure isotope shifts on the highly forbidden $^2S_{1/2} \rightarrow ^2F_{7/2}$ octupole transition of trapped $^{168,170,172,174,176}\text{Yb}$ ions. When combined with previous measurements in Yb^+ and very recent measurements in Yb , the data reveal a King plot nonlinearity of up to 240σ . The trends exhibited by experimental data are explained by nuclear density functional theory calculations with the Fayans functional. We also find, with 4.3σ confidence, that there is a second distinct source of nonlinearity, and discuss its possible origin.

DOI: [10.1103/PhysRevLett.128.163201](https://doi.org/10.1103/PhysRevLett.128.163201)

Despite ample evidence for the existence of dark matter [1–4] and concerted experimental searches for candidate particles [5–8], its origin and composition remain unknown. Isotope-shift (IS) spectroscopy has been recently proposed as a tabletop method to search for dark-matter candidates in the intermediate mass range $\lesssim 100 \text{ MeV}/c^2$ [9,10]. In particular, IS spectroscopy can be used to search for a hypothetical new boson, ϕ , that mediates interactions between quarks and leptons. An observable consequence is an additional isotope shift that arises from the effective interaction between neutrons and electrons. Such a shift could be detected as a deviation from linearity in a King plot [11] that compares the normalized isotope shifts for two different transitions. If at least three isotope shifts in each transition are measured, a deviation from linearity can be detected. The nonlinearity can also be caused by higher-order nuclear effects [12–18].

In our previous work, we reported evidence, at the 3σ level, for a nonlinearity in a King plot that compared two optical quadrupole transitions ($^2S_{1/2} \rightarrow ^2D_{3/2}$, $^2D_{5/2}$) in a trapped Yb^+ ion [19]. The measurement was performed for five even isotopes, one more than required, and we also proposed a new method to assign the nonlinearity to different possible physical origins based on the observed nonlinearity pattern. At the reported measurement accuracy of $\sim 300 \text{ Hz}$ on two relatively similar electronic excited

states, the source of the nonlinearity could not be discriminated, and was consistent both with a new boson and with standard-model (SM) nuclear shifts. IS spectroscopy in Ca^+ , which has lighter nuclei and therefore lower sensitivity to both new physics and nuclear effects than Yb^+ [10], showed no King nonlinearity at the 20 Hz level [20]. At the time of completion of the present work, large King nonlinearities were also reported when comparing transitions in neutral Yb [21,22] with the quadrupole transitions in Yb^+ .

In this Letter, we report IS laser spectroscopy for the highly forbidden octupole transition $^2S_{1/2} \rightarrow ^2F_{7/2}$ in Yb^+ . The electron configuration in the F state is very different from the previously measured D states [19], which increased the size of the observed King nonlinearity 20-fold (see Fig. 1). At a measurement resolution of $\sim 500 \text{ Hz}$, we observe a King-plot nonlinearity with 41 standard deviations σ . Including the recent data for neutral Yb [21,22] into our analysis, the significance of the nonlinearity rises to 240σ , and analyzing the patterns [19] we show that the measurements can be consistently explained by microscopic calculations carried out within nuclear density functional theory (DFT), which provides agreement with ground-state properties of complex deformed Yb isotopes [16,23]. Combining all measured transitions in Yb^+ and Yb , we further find evidence, at the

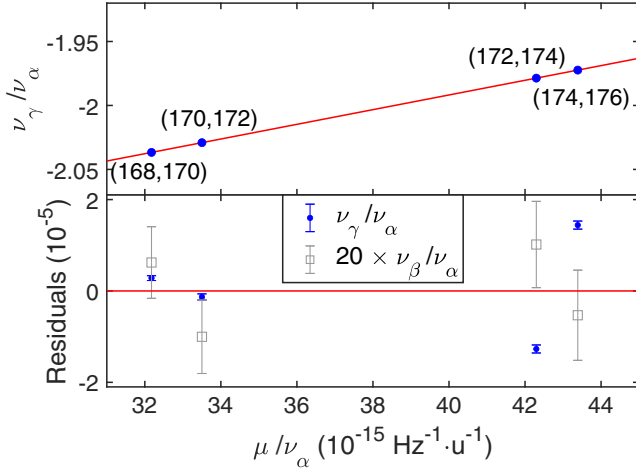


FIG. 1. Frequency-normalized King plot (top) and residuals (bottom, blue) for the γ ($^2S_{1/2} \rightarrow ^2F_{7/2}$) transition and reference transition α ($^2S_{1/2} \rightarrow ^2D_{5/2}$) for even-neighbor pairs ($A' = A + 2$) of Yb^+ isotopes. A deviation from linearity (red line) by 41 standard deviations σ is observed. For reference, residuals for the β ($^2S_{1/2} \rightarrow ^2D_{3/2}$) transition [19], magnified 20-fold, are also plotted in gray. The error bars indicate 2σ uncertainties; for correlations between the errors, see Supplemental Material [24].

4.3σ level, of a second, smaller source of nonlinearity, and discuss implications for limits on a new boson. Finally, we also extract nuclear data that can be used to further fine-tune nuclear energy density functionals.

Our IS measurements are performed on individual cold trapped $^A\text{Yb}^+$ ions with zero nuclear spin ($A \in \{168, 170, 172, 174, 176\}$). To make an IS measurement on the octupole transition $^2S_{1/2} \rightarrow ^2F_{7/2}$ near 467 nm that we label γ , we first load a single ion of one isotope A into the trap, Doppler cool it to $\sim 500 \mu\text{K}$, and measure the excitation probability when scanning the frequency of our probe laser, a frequency-doubled Ti:sapphire laser that is locked to an ultralow-thermal-expansion (ULE) cavity with linewidth $\kappa_c/(2\pi) = 30 \text{ kHz}$. We measure two transitions between Zeeman sublevels that are symmetrically detuned from the zero-field transition ν_γ , and determine the center frequency ν_γ^A as the mean (see Supplemental

Material [24]). A second isotope A' is then loaded into the trap and its center frequency $\nu_\gamma^{A'}$ is measured. We alternate several times between the two isotopes, achieving an accuracy of $\sim 500 \text{ Hz}$ in our measurement of the IS $\nu_\gamma^{AA'} \equiv \nu_\gamma^A - \nu_\gamma^{A'}$, limited mainly by the long-term stability of the ULE cavity. Our measured ISs $\nu_\gamma^{AA'}$ are given in Table I. Table II lists the absolute transition frequencies derived from our measured IS in combination with the absolute transition frequency for $^{172}\text{Yb}^+$ [56].

To a very good approximation, the IS can be factored into an electronic component, which is transition dependent (labeled by a greek letter subscript) but does not depend on the isotope, and a nuclear contribution, which depends on the isotopes (labeled by AA') but not on the electronic transition [9,11,14,19]:

$$\begin{aligned} \nu_\gamma^{AA'} = & F_\gamma \delta \langle r^2 \rangle^{AA'} + K_\gamma \mu^{AA'} + G_\gamma^{(4)} \delta \langle r^4 \rangle^{AA'} \\ & + G_\gamma^{(2)} [\delta \langle r^2 \rangle^2]^{AA'} + v_{ne} D_\gamma a^{AA'} + \dots \end{aligned} \quad (1)$$

Here $\delta \langle r^n \rangle^{AA'} \equiv \langle r^n \rangle^A - \langle r^n \rangle^{A'}$ is the difference in the n th nuclear charge moment between isotopes A and A' , $\mu^{AA'} \equiv 1/m^A - 1/m^{A'}$ is the inverse-mass difference, and $[\delta \langle r^2 \rangle^2]^{AA'} \equiv (\delta \langle r^2 \rangle^{AA''})^2 - (\delta \langle r^2 \rangle^{A'A''})^2$, with A'' denoting a reference isotope (we use $A'' = 172$). The quantity $v_{ne} = (-1)^{s+1} y_n y_e / (4\pi \hbar c)$ is the product of the coupling constants of the new boson to the neutron y_n and electron y_e , resulting in a Yukawa-like potential given by $V_{ne}(r) = \hbar c v_{ne} \exp(-r/\lambda_c)/r$ for a boson with spin s , mass m_ϕ , and reduced Compton wavelength $\lambda_c = \hbar/(m_\phi c)$ [9,14,19]. $a^{AA'} = A - A'$ is the neutron-number difference between the two isotopes. The coefficients F , K , $G^{(4)}$, $G^{(2)}$, and D are transition-dependent quantities that quantify the field shift, the mass shift, the fourth-moment shift, the quadratic field shift (QFS), and the sensitivity to the new boson, respectively.

To eliminate the large field shift F (associated with the size change of the nucleus $\delta \langle r^2 \rangle$, of order $\sim 4 \text{ GHz}$), and mass shift K (of order $\sim 0.2 \text{ GHz}$) contributions, one can use a second set of isotope shifts measured on a different

TABLE I. Isotope shifts $\nu_\gamma^{AA'} = \nu_\gamma^A - \nu_\gamma^{A'}$ measured for the $\gamma: ^2S_{1/2} \rightarrow ^2F_{7/2}$ (this work) and $\alpha: ^2S_{1/2} \rightarrow ^2D_{5/2}$ [19] transitions for pairs (A, A') of stable Yb^+ even isotopes. Inverse-mass differences $\mu^{AA'} = 1/m^A - 1/m^{A'}$ calculated from [57–60] with the Yb ionization energy set to 6.254 eV are also listed. Numbers in parentheses indicate 1σ statistical uncertainties.

(A, A')	$\nu_\gamma^{AA'}$ [MHz]	$\nu_\alpha^{AA'}$ [MHz]	$\mu^{AA'}$ [10^{-6} u^{-1}]
(168,170)	−4 438.160 30(50)	2 179.098 93(21)	70.113 619 5(36)
(170,172)	−4 149.190 38(45)	2 044.854 78(34)	68.506 890 49(63)
(172,174)	−3 132.321 60(50)	1 583.068 42(36)	66.958 651 95(64)
(174,176)	−2 976.391 60(48)	1 509.055 29(28)	65.474 078 21(65)
(168,172)	−8 587.352 00(47)		
(170,174)	−7 281.511 88(45)	3 627.922 95(50)	
(172,176)	−6 108.712 93(44)		

TABLE II. Absolute frequencies of the $\gamma: {}^2S_{1/2} \rightarrow {}^2F_{7/2}$ transition extracted from our IS measurements and the absolute frequency measurement in Refs. [56].

Isotope	Absolute frequency [THz]	Ref.
168	642.108 197 799 37(37)	[This work]
170	642.112 635 960 22(32)	[This work]
172	642.116 785 150 887 6(24)	[56]
174	642.119 917 472 26(33)	[This work]
176	642.122 893 863 84(36)	[This work]

reference transition τ to generate a King plot [11]. In its frequency-normalized version [19], the relationship studied can be written as

$$\bar{\nu}_\gamma^{AA'} = f_{\gamma\tau} + K_{\gamma\tau} \bar{\mu}^{AA'} + G_{\gamma\tau}^{(4)} \overline{\delta\langle r^4 \rangle}^{AA'} + G_{\gamma\tau}^{(2)} \overline{[\delta\langle r^2 \rangle]^2}^{AA'} + v_{ne} D_{\gamma\tau} \bar{a}^{AA'}, \quad (2)$$

where the notation $\bar{x}^{AA'} \equiv x^{AA'}/\nu_\tau^{AA'}$ indicates frequency-normalized terms. We define $z_{\gamma\tau} \equiv Z_\gamma/Z_\tau$ as the ratio of coefficients for transitions γ and τ , and $Z_{\gamma\tau} \equiv Z_\gamma(1 - f_{\gamma\tau}/z_{\gamma\tau})$ for $Z \in \{F, K, G^{(2)}, G^{(4)}, D\}$. The first two terms in Eq. (2) represent the linear relation between $\bar{\nu}_\gamma$ and $\bar{\mu}$ in the King plot, while the remaining terms possibly violate the linearity.

Figure 1 shows a frequency-normalized King plot using the previously measured transition $\alpha: {}^2S_{1/2} \rightarrow {}^2D_{5/2}$ near 411 nm [19] as the reference transition τ . The residuals from the linear fit reveal a nonlinearity at the 10^{-5} level, corresponding to 41σ . The nonlinearity is 20 times larger than the nonlinearity we observed previously [19] comparing the two quadrupole transitions, α and $\beta: {}^2S_{1/2} \rightarrow {}^2D_{3/2}$, that have a more similar electronic structure. The recent measurements in neutral Yb [21,22], when combined with our α or β transition data, confirm a nonlinearity of a similar size (see also Fig. 2).

Having unambiguously established a King nonlinearity, we can gain information about the sources of nonlinearity by analyzing the deviation patterns [19]. With four isotope-shift data points, we can rewrite Eq. (2) in terms of four-dimensional vectors as follows:

$$\bar{\nu}_\gamma = f_{\gamma\tau} \mathbf{1} + K_{\gamma\tau} \bar{\boldsymbol{\mu}} + (\lambda_+ \boldsymbol{\Lambda}_+ + \lambda_- \boldsymbol{\Lambda}_-), \quad (3)$$

where the vector space inhabited by the vectors $z \equiv (z_1, z_2, z_3, z_4)$ with $z_k \equiv z^{A, A+2}$ ($A = 166 + 2k$ for $k = 1, 2, 3, 4$, $z \in \{\bar{\boldsymbol{\mu}}, \bar{\boldsymbol{\nu}}_\gamma\}$) is spanned by the basis $(\mathbf{1}, \bar{\boldsymbol{\mu}}, \boldsymbol{\Lambda}_+, \boldsymbol{\Lambda}_-)$.

The first two vectors, $\mathbf{1} \equiv (1, 1, 1, 1)$ and $\bar{\boldsymbol{\mu}}$, define a plane of King linearity (i.e., the component of $\bar{\boldsymbol{\nu}}_\gamma$ in this plane does not give rise to King nonlinearities), while the unit vectors $\boldsymbol{\Lambda}_+$ and $\boldsymbol{\Lambda}_-$, defined as $\boldsymbol{\Lambda}_+ \propto (\bar{\mu}_3 - \bar{\mu}_2, \bar{\mu}_1 - \bar{\mu}_4, \bar{\mu}_4 - \bar{\mu}_1, \bar{\mu}_2 - \bar{\mu}_3)$ and $\boldsymbol{\Lambda}_- \propto (\bar{\mu}_4 - \bar{\mu}_2, \bar{\mu}_1 - \bar{\mu}_3, \bar{\mu}_2 - \bar{\mu}_4, \bar{\mu}_3 - \bar{\mu}_1)$, span the out-of-plane space of vectors that produce a

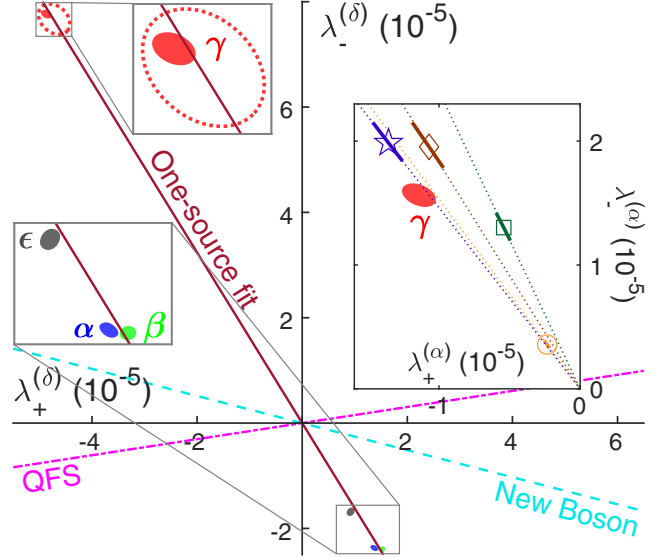


FIG. 2. Decomposition of the measured nonlinearity (solid ellipses, 95% confidence interval) onto the (λ_+, λ_-) basis for the transitions $\alpha: {}^2S_{1/2} \rightarrow {}^2D_{5/2}$ in Yb⁺ (blue) [19], $\beta: {}^2S_{1/2} \rightarrow {}^2D_{3/2}$ in Yb⁺ (green) [19], $\epsilon: {}^1S_0 \rightarrow {}^1D_2$ (dark gray) in Yb [22], and $\gamma: {}^2S_{1/2} \rightarrow {}^2F_{7/2}$ in Yb⁺ (red, this work). The corresponding frequency-normalized King plot is generated with the reference transition $\delta: {}^1S_0 \rightarrow {}^3P_0$ in Yb [21] ($\lambda_{\pm}^{(\delta)}$) that has been measured with the highest frequency accuracy. The red dotted ellipse indicates a previous preliminary measurement for the γ transition [61]. The dashed lines indicate the ratio λ_+/λ_- that would arise solely from a new boson (light blue dashed line) or the QFS (pink dash-dotted line). The brown solid line is a single-source fit to all four transitions $\alpha, \beta, \gamma, \epsilon$, yielding evidence for a second nonlinearity source with 4.3σ significance ($\chi^2 = 25.4$). The largest inset shows the nonlinearity in a King plot with α as the reference transition ($\lambda_{\pm}^{(\alpha)}$). Open symbols indicate the nonlinearity due to $\delta\langle r^4 \rangle^{AA'}$ from nuclear DFT calculations with SV-min (square), RD-min (diamond), UNEDF1 (circle), and Fy(Δr) (star) energy density functionals. Short bold lines indicate the uncertainty in electronic-structure calculations (see Supplemental Material [24]).

King nonlinearity (see Supplemental Material [24]). Any vector with nonzero residuals from the linear King plot fit hence has components in the space spanned by $(\boldsymbol{\Lambda}_+, \boldsymbol{\Lambda}_-)$, and can be expressed in terms of its scalar components λ_+ and λ_- along $\boldsymbol{\Lambda}_+$ and $\boldsymbol{\Lambda}_-$, respectively. $(\boldsymbol{\Lambda}_+$ and $\boldsymbol{\Lambda}_-$ correspond approximately to the zigzag $+-+-$ and curved $+-+-$ patterns of residuals introduced in Ref. [19].) Both SM and new-boson effects produce nonlinearities with a defined λ_+/λ_- ratio, given by the associated nuclear factors $x^{AA'}$, and are characterized by lines along definite directions in the λ_{\pm} plane (see Fig. 2).

Figure 2 displays the measured nonlinearity in the λ_{\pm} plane for the γ transition, as well as for the previously measured α and β transitions in Yb⁺ [19], and the recently measured $\epsilon: {}^1S_0 \rightarrow {}^1D_2$ transition in Yb [22]. For the reference transition τ in Eq. (2), we choose in Fig. 2 the

transition $\delta: ^1S_0 \rightarrow ^3P_0$ in Yb that has been very recently measured with the highest frequency accuracy [21]. All measured transitions $\alpha, \beta, \gamma, \epsilon, \delta$ are consistent with each other in that they lie nearly along the same direction in the λ_{\pm} plane, indicating that the nonlinearity originates from a common dominant source for all transitions. This direction corresponds neither to a new boson $a^{AA'}$ nor to the QFS $[\delta\langle r^2 \rangle^2]^{AA'}$.

To interpret the IS measurements, we performed quantified nuclear calculations of $\langle r^2 \rangle$ and $\langle r^4 \rangle$ using nuclear density functional theory (DFT) with realistic energy density functionals (EDFs). The nuclear charge radial moments were obtained directly from calculated charge densities as discussed in Refs. [16,23]. To explore a possible span of predictions, we consider four different EDFs: Skyrme functionals SV-min and UNEDF1, extended Skyrme functional RD-min, and the Fayans functional $Fy(\Delta r)$. The calculated $\delta\langle r^4 \rangle$ are multiplied by $G_{\gamma\alpha}^{(4)}$ from atomic structure calculations to predict the nonlinearity for $G_{\gamma\alpha}^{(4)}\delta\langle r^4 \rangle$. For details on the calculations, see Refs. [62,63] and Supplemental Material [24].

The predicted values of $\langle r^2 \rangle$ and $\langle r^4 \rangle$ are impacted by several effects [16,23,64,65], including the surface thickness of nuclear density that shows a pronounced particle-number dependence due to shell effects; the relativistic corrections that contain contributions from the intrinsic nucleon form factors; and nuclear deformation and pairing effects, which also give rise to the fragmentation [23] of the single-particle spin-orbit strength that affects spin-orbit contributions to charge moments. Our DFT calculations take all these effects into account. In this respect, a King plot nonlinearity may be rooted in several nuclear structure effects impacting $\langle r^2 \rangle$ and $\langle r^4 \rangle$, not just one as discussed in Ref. [13]. As shown in the large inset to Fig. 2, our DFT results agree well with the observed direction in the λ_{\pm} plane (see Supplemental Material [24] for details).

We can also directly compare the calculated changes in the nuclear size $\delta\langle r^2 \rangle$ to the measured values. In order to be insensitive to the electronic factor F in Eq. (1), which can currently only be calculated with a typical uncertainty of $\lesssim 30\%$, we plot in Fig. 3(a) the ratios $\delta\langle r^2 \rangle^{A,A+2}/\delta\langle r^2 \rangle^{A-2,A}$ that can be determined from the experimental data with much higher accuracy. The nuclear calculations agree with the IS data to within 20%. The ratios obtained from nuclear theory show monotonically increasing trends for the three EDFs SV-min, RD-min, and UNEDF1. Only $Fy(\Delta r)$ produces a trend that is consistent with data. This is yet another demonstration that the Fayans functional is better adapted to local nonmonotonic trends in charge radius data, see also Refs. [66–68]. We note that $Fy(\Delta r)$ also provides a better description of nuclear quadrupole deformations as compared to other EDFs, see Supplemental Material [24] for details. This demonstrates that high-precision data on

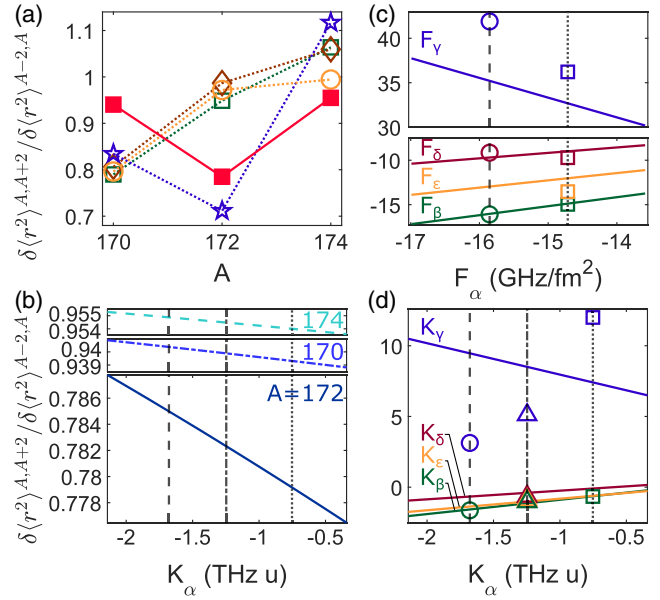


FIG. 3. (a) Comparison plot of derived values for the ratio of the mean-square nuclear radius differences between $(A, A+2)$ isotope pairs. Open symbols mark the values derived from nuclear calculations using SV-min, RD-min, UNEDF1, and $Fy(\Delta r)$ energy density functionals (see Fig. 2 for symbol assignments). The red filled square symbols are values derived from measured ISs on the 411 nm transition in combination with mass shifts from configuration interaction (CI) [69–72] calculations. (b) Plot of derived values for the ratio of the mean square nuclear radius between sequential isotope pairs as a function of K_{α} , showing very weak dependence on K_{α} . (c),(d) Derived values of $F_{\beta}, F_{\gamma}, F_{\delta}, F_{\epsilon}$ ($K_{\beta}, K_{\gamma}, K_{\delta}, K_{\epsilon}$) as a function of F_{α} (K_{α}), using the experimentally determined ratios $F_{\kappa\alpha}$ ($K_{\kappa\alpha}$) for $\kappa = \beta, \gamma, \delta, \epsilon$. In (b), (c), and (d), dashed (dotted) vertical lines and round (square) markers indicate values from CI calculations using GRASP2018 [73] (AMBiT [74]). Dash-dotted lines and open triangle markers correspond to CI and many-body perturbation theory (CI + MBPT) [75] calculations using AMBiT.

nuclear radii deliver important information for discrimination and further development of nuclear models.

Our data also provide strong tests for electronic-structure calculations, as shown in Figs. 3(c) and 3(d): The field (mass) shift coefficient F_{τ} (K_{τ}) on one transition τ determines the coefficients on all other transitions κ via the experimentally determined value of $F_{\kappa\tau}$ ($K_{\kappa\tau}$) (see Supplemental Material [24] for details).

While all transitions $\alpha, \beta, \gamma, \epsilon$ lie near a line through the origin in Fig. 2, there is a deviation from that line for all four transitions (plus the reference transition δ) with 4.3σ significance. (In contrast, the generalized King plot proposed in previous studies [14,76] provides a test only for three transitions, giving significance less than 4σ for any choices of three transitions; see Supplemental Material [24]). This second nonlinearity is too large to be explained by the QFS, which is expected to be the next largest source of nonlinearity within the SM (see

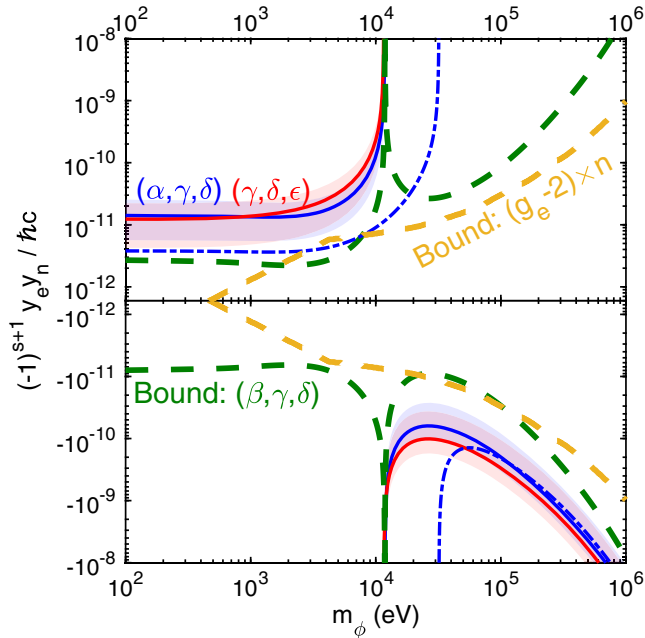


FIG. 4. Product of coupling constants $y_e y_n$ of a new boson with spin s versus boson mass m_ϕ , derived from generalized-King-plot analyses [14,76] of groups of three transitions (α, γ, δ) (blue), $(\gamma, \delta, \epsilon)$ (red), and (β, γ, δ) (green), assuming that the observed second nonlinearity is dominated by a new boson. Dashed lines indicate the lower bounds of $y_e y_n$'s excluded magnitude. Solid lines and shaded areas are center values and confidence intervals for configuration-interaction calculations using AMBIT. [we show the $\approx 95\%$ confidence interval (see Supplemental Material [24]) that arises from the statistical uncertainty in the measured ISs. The systematic uncertainty due to the atomic structure calculations is larger; the dash-dotted line shows the center value of $y_e y_n$ for the (α, γ, δ) transition combination using GRASP2018 calculation results, for comparison.] The yellow line indicates the bound derived from electron $g_e - 2$ measurements [77–80] in combination with neutron scattering measurements [81–84] from Ref. [10].

Supplemental Material [24]). In Fig. 4, we show the strength of the coupling constant $y_e y_n$ for a new boson vs boson mass under the assumption that the new boson is the sole source of the second nonlinearity. Different combinations of measured transitions give similar values or bounds for the coupling strength $y_e y_n$ that is near or slightly exceeds the best other laboratory bounds given by the combination of $g - 2$ measurements on the electron and neutron scattering experiments [10,77–84].

In the future, it should be possible to reduce the experimental uncertainties by up to 4 orders of magnitude to sub-Hz levels, as has been demonstrated with simultaneously trapped Sr^+ ions [85]. In combination with improved electronic and nuclear calculations, it should then be possible to determine unambiguously if some part of the observed nonlinearity cannot be explained by physics within the SM. Besides better measurements on (more) transitions, it may also become possible to perform

further measurements on unstable isotopes, which would allow the direct extraction (and elimination) of additional nuclear effects.

This work was supported by the NSF CUA and the U.S. Department of Energy, Office of Science, Office of Nuclear Physics under Grants No. DE-SC0013365 and No. DE-SC0018083 (NUCLEI SciDAC-4 collaboration). This project has received funding from the European Union's Horizon 2020 research and innovation programme under the Marie Skłodowska-Curie Grant Agreement No. 795121. J.C.B. is supported by the Australian Research Council (DP190100974). C.L. was supported by the U.S. Department of Defense (DOD) through the National Defense Science and Engineering Graduate Fellowship (NDSEG) Program.

*These authors contributed equally to this work.

†vuletic@mit.edu

- [1] V. C. Rubin, W. K. Ford, and N. Thonnard, Rotational properties of 21 Sc galaxies with a large range of luminosities and radii, from NGC 4605 ($R = 4$ kpc) to UGC 2885 ($R = 122$ kpc), *Astrophys. J.* **238**, 471 (1980).
- [2] D. Clowe, M. Bradač, A. H. Gonzalez, M. Markevitch, S. W. Randall, C. Jones, and D. Zaritsky, A direct empirical proof of the existence of dark matter, *Astrophys. J.* **648**, L109 (2006).
- [3] R. Massey, T. Kitching, and J. Richard, The dark matter of gravitational lensing, *Rep. Prog. Phys.* **73**, 086901 (2010).
- [4] N. Aghanim *et al.* (Planck Collaboration), Planck 2018 results—I. Overview and the cosmological legacy of Planck, *Astron. Astrophys.* **641**, A1 (2020).
- [5] P. Zyla *et al.* (Particle Data Group), Review of particle physics, *Prog. Theor. Exp. Phys.* **2020**, 083C01 (2020).
- [6] K. Choi, S. H. Im, and C. S. Shin, Recent progress in the physics of axions and axion-like particles, *Annu. Rev. Nucl. Part. Sci.* **71**, 225 (2021).
- [7] T. E. Chupp, P. Fierlinger, M. J. Ramsey-Musolf, and J. T. Singh, Electric dipole moments of atoms, molecules, nuclei, and particles, *Rev. Mod. Phys.* **91**, 015001 (2019).
- [8] M. S. Safronova, D. Budker, D. DeMille, Derek F. Jackson Kimball, A. Derevianko, and C. W. Clark, Search for new physics with atoms and molecules, *Rev. Mod. Phys.* **90**, 025008 (2018).
- [9] C. Delaunay, R. Ozeri, G. Perez, and Y. Soreq, Probing atomic Higgs-like forces at the precision frontier, *Phys. Rev. D* **96**, 093001 (2017).
- [10] J. C. Berengut, D. Budker, C. Delaunay, V. V. Flambaum, C. Fruguele, E. Fuchs, C. Grojean, R. Harnik, R. Ozeri, G. Perez, and Y. Soreq, Probing New Long-Range Interactions by Isotope Shift Spectroscopy, *Phys. Rev. Lett.* **120**, 091801 (2018).
- [11] W. H. King, *Isotope Shifts in Atomic Spectra* (Springer Science+Business Media, LLC, New York, 1984), 10.1007/978-1-4899-1786-7.
- [12] V. V. Flambaum, A. J. Geddes, and A. V. Viatkina, Isotope shift, nonlinearity of King plots, and the search for new particles, *Phys. Rev. A* **97**, 032510 (2018).

- [13] S. O. Allehabi, V. A. Dzuba, V. V. Flambaum, and A. V. Afanasjev, Nuclear deformation as a source of the non-linearity of the King plot in the Yb^+ ion, *Phys. Rev. A* **103**, L030801 (2021).
- [14] K. Mikami, M. Tanaka, and Y. Yamamoto, Probing new intra-atomic force with isotope shifts, *Eur. Phys. J. C* **77**, 896 (2017).
- [15] M. Tanaka and Y. Yamamoto, Relativistic effects in the search for new intra-atomic force with isotope shifts, *Prog. Theor. Exp. Phys.* **2020**, 103B02 (2020).
- [16] P.-G. Reinhard, W. Nazarewicz, and R. F. Garcia Ruiz, Beyond the charge radius: The information content of the fourth radial moment, *Phys. Rev. C* **101**, 021301(R) (2020).
- [17] S. O. Allehabi, V. A. Dzuba, V. V. Flambaum, A. V. Afanasjev, and S. E. Agbemava, Using isotope shift for testing nuclear theory: The case of nobelium isotopes, *Phys. Rev. C* **102**, 024326 (2020).
- [18] R. A. Müller, V. A. Yerokhin, A. N. Artemyev, and A. Surzhykov, Nonlinearities of King's plot and their dependence on nuclear radii, *Phys. Rev. A* **104**, L020802 (2021).
- [19] I. Counts, J. Hur, D. P. L. Aude Craik, H. Jeon, C. Leung, J. C. Berengut, A. Geddes, A. Kawasaki, W. Jhe, and V. Vuletić, Evidence for Nonlinear Isotope Shift in Yb^+ Search for New Boson, *Phys. Rev. Lett.* **125**, 123002 (2020).
- [20] C. Solaro, S. Meyer, K. Fisher, J. C. Berengut, E. Fuchs, and M. Drewsen, Improved Isotope-Shift-Based Bounds on Bosons beyond the Standard Model through Measurements of the $^2D_{3/2} - ^2D_{5/2}$ Interval in Ca^+ , *Phys. Rev. Lett.* **125**, 123003 (2020).
- [21] K. Ono, Y. Saito, T. Ishiyama, T. Higomoto, T. Takano, Y. Takasu, Y. Yamamoto, M. Tanaka, and Y. Takahashi, Observation of non-linearity of generalized King plot in the search for new boson, [arXiv:2110.13544](https://arxiv.org/abs/2110.13544) [Phys. Rev. X].
- [22] N. L. Figueroa, J. C. Berengut, V. A. Dzuba, V. V. Flambaum, D. Budker, and D. Antypas, Precision Determination of Isotope Shifts in Ytterbium and Implications for New Physics, *Phys. Rev. Lett.* **128**, 073001 (2022).
- [23] P.-G. Reinhard and W. Nazarewicz, Nuclear charge densities in spherical and deformed nuclei: Toward precise calculations of charge radii, *Phys. Rev. C* **103**, 054310 (2021).
- [24] See Supplemental Material at <http://link.aps.org/supplemental/10.1103/PhysRevLett.128.163201> for the details on experimental protocols, data analysis, estimation of systematic effects, and the calculation of electronic factors and nuclear parameters, which includes Refs. [25–55].
- [25] M. Aymar, A. Debarre, and O. Robaux, Highly excited levels of neutral ytterbium. II. Multichannel quantum defect analysis of odd- and even-parity spectra, *J. Phys. B* **13**, 1089 (1980).
- [26] M. Bender, P.-H. Heenen, and P.-G. Reinhard, Self-consistent mean-field models for nuclear structure, *Rev. Mod. Phys.* **75**, 121 (2003).
- [27] J. C. Berengut, V. A. Dzuba, and V. V. Flambaum, Isotope-shift calculations for atoms with one valence electron, *Phys. Rev. A* **68**, 022502 (2003).
- [28] P. Bogdanovich and G. Žukauskas, Approximate allowance for superposition of configurations in atomic spectra, *Sov. Phys. Collect.* **23**, 13 (1983).
- [29] K. Dyall, I. Grant, C. Johnson, F. Parpia, and E. Plummer, GRASP: A general-purpose relativistic atomic structure program, *Comput. Phys. Commun.* **55**, 425 (1989).
- [30] C. L. Edmunds, T. R. Tan, A. R. Milne, A. Singh, M. J. Biercuk, and C. Hempel, Scalable hyperfine qubit state detection via electron shelving in the $^2D_{5/2}$ and $^2F_{7/2}$ manifolds in $^{171}\text{Yb}^+$, *Phys. Rev. A* **104**, 012606 (2021).
- [31] J. Ekman, P. Jönsson, M. Godefroid, C. Nazé, G. Gaigalas, and J. Bieroń, RIS4: A program for relativistic isotope shift calculations, *Comput. Phys. Commun.* **235**, 433 (2019).
- [32] J. Erler, P. Klüpfel, and P.-G. Reinhard, Exploration of a modified density dependence in the Skyrme functional, *Phys. Rev. C* **82**, 044307 (2010).
- [33] I. Grant, B. McKenzie, P. Norrington, D. Mayers, and N. Pyper, An atomic multiconfigurational Dirac-Fock package, *Comput. Phys. Commun.* **21**, 207 (1980).
- [34] N. Huntemann, M. Okhapkin, B. Lipphardt, S. Weyers, C. Tamm, and E. Peik, High-Accuracy Optical Clock Based on the Octupole Transition in $^{171}\text{Yb}^+$, *Phys. Rev. Lett.* **108**, 090801 (2012).
- [35] Y.-Y. Jau, J. D. Hunker, and P. D. D. Schwindt, F-state quenching with CH_4 for buffer-gas cooled $^{171}\text{Yb}^+$ frequency standard, *AIP Adv.* **5**, 117209 (2015).
- [36] S. A. King, R. M. Godun, S. A. Webster, H. S. Margolis, L. A. M. Johnson, K. Szymaniec, P. E. G. Baird, and P. Gill, Absolute frequency measurement of the $^2S_{1/2} - ^2F_{7/2}$ electric octupole transition in a single ion of $^{171}\text{Yb}^+$ with 10^{-15} fractional uncertainty, *New J. Phys.* **14**, 013045 (2012).
- [37] M. Kortelainen, J. McDonnell, W. Nazarewicz, P.-G. Reinhard, J. Sarich, N. Schunck, M. V. Stoitsov, and S. M. Wild, Nuclear energy density optimization: Large deformations, *Phys. Rev. C* **85**, 024304 (2012).
- [38] J. J. McLoughlin, A. H. Nizamani, J. D. Siverns, R. C. Sterling, M. D. Hughes, B. Lekitsch, B. Stein, S. Weidt, and W. K. Hensinger, Versatile ytterbium ion trap experiment for operation of scalable ion-trap chips with motional heating and transition-frequency measurements, *Phys. Rev. A* **83**, 013406 (2011).
- [39] S. Mulholland, H. A. Klein, G. P. Barwood, S. Donnellan, P. B. R. Nisbet-Jones, G. Huang, G. Walsh, P. E. G. Baird, and P. Gill, Compact laser system for a laser-cooled ytterbium ion microwave frequency standard, *Rev. Sci. Instrum.* **90**, 033105 (2019).
- [40] A. Kramida, Yu. Ralchenko, and J. Reader (NIST ASD Team), NIST Atomic Spectra Database (ver. 5.9), [Online]. Available: <https://physics.nist.gov/asd> (2021, November 2). National Institute of Standards and Technology, Gaithersburg, MD (2021).
- [41] S. Olmschenk, K. C. Younge, D. L. Moehring, D. N. Matsukevich, P. Maunz, and C. Monroe, Manipulation and detection of a trapped Yb^+ hyperfine qubit, *Phys. Rev. A* **76**, 052314 (2007).
- [42] A. Papoulia, B. G. Carlsson, and J. Ekman, Effect of realistic nuclear charge distributions on isotope shifts and progress towards the extraction of higher-order nuclear radial moments, *Phys. Rev. A* **94**, 042502 (2016).
- [43] M. Pizzocaro, F. Bregolin, P. Barbieri, B. Rauf, F. Levi, and D. Calonico, Absolute frequency measurement of the $^1S_0 - ^3P_0$ transition of ^{171}Yb with a link to international atomic time, *Metrologia* **57**, 035007 (2020).

- [44] B. Pritychenko, M. Birch, B. Singh, and M. Horoi, Tables of E2 transition probabilities from the first 2+ states in even-even nuclei, *At. Data Nucl. Data Tables* **107**, 1 (2016).
- [45] M. Puchalski and K. Pachucki, Nuclear structure effects in the isotope shift with halo nuclei, *Hyperfine Interact.* **196**, 35 (2010).
- [46] J. Hur, REDF (v1.0.0), Zenodo, [10.5281/zenodo.5818081](https://doi.org/10.5281/zenodo.5818081) (2022).
- [47] A. M. Ransford, Old dog, new trick: High fidelity, background-free state detection of an ytterbium ion qubit, Ph.D. thesis, The University of California, Los Angeles, 2020.
- [48] P.-G. Reinhard and W. Nazarewicz, Toward a global description of nuclear charge radii: Exploring the Fayans energy density functional, *Phys. Rev. C* **95**, 064328 (2017).
- [49] M. Roberts, P. Taylor, S. V. Gateva-Kostova, R. B. M. Clarke, W. R. C. Rowley, and P. Gill, Measurement of the $^2S_{1/2} - ^2D_{5/2}$ clock transition in a single $^{171}\text{Yb}^+$ ion, *Phys. Rev. A* **60**, 2867 (1999).
- [50] M. S. Safronova, M. G. Kozlov, and C. W. Clark, Blackbody radiation shifts in optical atomic clocks, *IEEE Trans. Ultrason. Ferroelectr. Freq. Control* **59**, 439 (2012).
- [51] K. Sugiyama, A. Wakita, and A. Nakata, Diode-laser-based light sources for laser cooling of trapped Yb^+ ions, in *Conference on Precision Electromagnetic Measurements. Conference Digest. CPEM 2000* (Cat. No. 00CH37031) (IEEE, Sydney, 2000), pp. 509–510, [10.1109/CPEM.2000.851105](https://doi.org/10.1109/CPEM.2000.851105).
- [52] C. Tamm, S. Weyers, B. Lipphardt, and E. Peik, Stray-field-induced quadrupole shift and absolute frequency of the 688-THz $^{171}\text{Yb}^+$ single-ion optical frequency standard, *Phys. Rev. A* **80**, 043403 (2009).
- [53] P. Taylor, M. Roberts, S. V. Gateva-Kostova, R. B. M. Clarke, G. P. Barwood, W. R. C. Rowley, and P. Gill, Investigation of the $^2S_{1/2} - ^2D_{5/2}$ clock transition in a single ytterbium ion, *Phys. Rev. A* **56**, 2699 (1997).
- [54] S. Webster, R. Godun, S. King, G. Huang, B. Walton, V. Tsaturian, H. Margolis, S. Lea, and P. Gill, Frequency measurement of the $^2S_{1/2} - ^2D_{3/2}$ electric quadrupole transition in a single $^{171}\text{Yb}^+$ ion, *IEEE Trans. Ultrason. Ferroelectr. Freq. Control* **57**, 592 (2010).
- [55] W. Zhang, M. J. Martin, C. Benko, J. L. Hall, J. Ye, C. Hagemann, T. Legero, U. Sterr, F. Riehle, G. D. Cole, and M. Aspelmeyer, Reduction of residual amplitude modulation to 1×10^{-6} for frequency modulation and laser stabilization, *Opt. Lett.* **39**, 1980 (2014).
- [56] H. A. FÜRST, C.-H. Yeh, D. Kalincev, A. P. Kulosa, L. S. Dreissen, R. Lange, E. Benkler, N. Huntemann, E. Peik, and T. E. Mehlstäubler, Coherent Excitation of the Highly Forbidden Electric Octupole Transition in $^{172}\text{Yb}^+$, *Phys. Rev. Lett.* **125**, 163001 (2020); **128**, 149901(E) (2020).
- [57] D. Nesterenko, R. de Groote, T. Eronen, Z. Ge, M. Hukkanen, A. Jokinen, and A. Kankainen, High-precision mass measurement of ^{168}Yb for verification of nonlinear isotope shift, *Int. J. Mass Spectrom.* **458**, 116435 (2020).
- [58] W. Huang, G. Audi, M. Wang, F. G. Kondev, S. Naimi, and X. Xu, The AME2016 atomic mass evaluation (I). Evaluation of input data; and adjustment procedures, *Chin. Phys. C* **41**, 030002 (2017).
- [59] M. Wang, G. Audi, F. G. Kondev, W. Huang, S. Naimi, and X. Xu, The AME2016 atomic mass evaluation (II). Tables, graphs and references, *Chin. Phys. C* **41**, 030003 (2017).
- [60] R. Rana, M. Höcker, and E. G. Myers, Atomic masses of strontium and ytterbium, *Phys. Rev. A* **86**, 050502(R) (2012).
- [61] I. Counts, Surface friction and spectroscopic probes of new physics with trapped ions, Ph.D. thesis, Massachusetts Institute of Technology, 2020.
- [62] P.-G. Reinhard, B. Schuettrumpf, and J. Maruhn, The axial Hartree-Fock + BCS code SkyAx, *Comput. Phys. Commun.* **258**, 107603 (2021).
- [63] P. Klüpfel, P.-G. Reinhard, T. J. Bürvenich, and J. A. Maruhn, Variations on a theme by Skyrme: A systematic study of adjustments of model parameters, *Phys. Rev. C* **79**, 034310 (2009).
- [64] B. A. Brown, C. R. Bronk, and P. E. Hodgson, Systematics of nuclear RMS charge radii, *J. Phys. G* **10**, 1683 (1984).
- [65] E. W. Otten, Nuclear radii and moments of unstable isotopes, in *Treatise on Heavy Ion Science: Volume 8: Nuclei Far From Stability*, edited by D. A. Bromley (Springer US, Boston, MA, 1989), pp. 517–638, [10.1007/978-1-4613-0713-6_7](https://doi.org/10.1007/978-1-4613-0713-6_7).
- [66] M. Hammen *et al.*, From Calcium to Cadmium: Testing the Pairing Functional through Charge Radii Measurements of $^{100-130}\text{Cd}$, *Phys. Rev. Lett.* **121**, 102501 (2018).
- [67] C. Gorges *et al.*, Laser Spectroscopy of Neutron-Rich Tin Isotopes: A Discontinuity in Charge Radii Across the $N = 82$ Shell Closure, *Phys. Rev. Lett.* **122**, 192502 (2019).
- [68] A. J. Miller, K. Minamisono, A. Klose, D. Garand, C. Kujawa, J. D. Lantis, Y. Liu, B. Maaß, P. F. Mantica, W. Nazarewicz, W. Nörtershäuser, S. V. Pineda, P.-G. Reinhard, D. M. Rossi, F. Sommer, C. Sumithrarachchi, A. Teigelhöfer, and J. Watkins, Proton superfluidity and charge radii in proton-rich calcium isotopes, *Nat. Phys.* **15**, 432 (2019).
- [69] P. Jönsson, A. Ynnerman, C. Froese Fischer, M. R. Godefroid, and J. Olsen, Large-scale multiconfiguration Hartree-Fock and configuration-interaction calculations of the transition probability and hyperfine structures in the sodium resonance transition, *Phys. Rev. A* **53**, 4021 (1996).
- [70] S. G. Porsev, M. G. Kozlov, and D. Reimers, Transition frequency shifts with fine-structure constant variation for Fe I and isotope-shift calculations in Fe I and Fe II, *Phys. Rev. A* **79**, 032519 (2009).
- [71] B. Fawcett and M. Wilson, Computed oscillator strengths, Landé g values, and lifetimes in Yb II, *At. Data Nucl. Data Tables* **47**, 241 (1991).
- [72] E. Biémont, J.-F. Dutrieux, I. Martin, and P. Quinet, Lifetime calculations in Yb II, *J. Phys. B* **31**, 3321 (1998).
- [73] C. Froese Fischer, G. Gaigalas, P. Jönsson, and J. Bieroń, GRASP2018—a Fortran 95 version of the general relativistic atomic structure package, *Comput. Phys. Commun.* **237**, 184 (2019).
- [74] E. Kahl and J. Berengut, AMBiT: A programme for high-precision relativistic atomic structure calculations, *Comput. Phys. Commun.* **238**, 232 (2019).

- [75] V. A. Dzuba, V. V. Flambaum, and M. G. Kozlov, Combination of the many-body perturbation theory with the configuration-interaction method, *Phys. Rev. A* **54**, 3948 (1996).
- [76] J. C. Berengut, C. Delaunay, A. Geddes, and Y. Soreq, Generalized King linearity and new physics searches with isotope shifts, *Phys. Rev. Research* **2**, 043444 (2020).
- [77] D. Hanneke, S. Fogwell, and G. Gabrielse, New Measurement of the Electron Magnetic Moment and the Fine Structure Constant, *Phys. Rev. Lett.* **100**, 120801 (2008).
- [78] T. Aoyama, M. Hayakawa, T. Kinoshita, and M. Nio, Tenth-Order QED Contribution to the Electron $g - 2$ and an Improved Value of the Fine Structure Constant, *Phys. Rev. Lett.* **109**, 111807 (2012).
- [79] R. Bouchendira, P. Cladé, S. Guellati-Khélifa, F. Nez, and F. Biraben, New Determination of the Fine Structure Constant and Test of the Quantum Electrodynamics, *Phys. Rev. Lett.* **106**, 080801 (2011).
- [80] H. Davoudiasl, H.-S. Lee, and W. J. Marciano, Muon $g - 2$, rare kaon decays, and parity violation from dark bosons, *Phys. Rev. D* **89**, 095006 (2014).
- [81] R. Barbieri and T. Ericson, Evidence against the existence of a low mass scalar boson from neutron-nucleus scattering, *Phys. Lett.* **57B**, 270 (1975).
- [82] H. Leeb and J. Schmiedmayer, Constraint on Hypothetical Light Interacting Bosons from Low-Energy Neutron Experiments, *Phys. Rev. Lett.* **68**, 1472 (1992).
- [83] Y. N. Pokotilovski, Constraints on new interactions from neutron scattering experiments, *Phys. At. Nucl.* **69**, 924 (2006).
- [84] V. V. Nesvizhevsky, G. Pignol, and K. V. Protasov, Neutron scattering and extra-short-range interactions, *Phys. Rev. D* **77**, 034020 (2008).
- [85] T. Manovitz, R. Shaniv, Y. Shapira, R. Ozeri, and N. Akerman, Precision Measurement of Atomic Isotope Shifts Using a Two-Isotope Entangled State, *Phys. Rev. Lett.* **123**, 203001 (2019).